

Nonlinear dendritic processing determines angular tuning of barrel cortex neurons *in vivo*

Maria Lavzin^{1*}, Sophia Rapoport^{1*}, Alon Polsky², Liora Garion¹ & Jackie Schiller¹

Layer 4 neurons in primary sensory cortices receive direct sensory information from the external world^{1,2}. A general feature of these neurons is their selectivity to specific features of the sensory stimulation³⁻⁵. Various theories try to explain the manner in which these neurons are driven by their incoming sensory information⁶⁻¹¹. In all of these theories neurons are regarded as simple elements summing small biased inputs to create tuned output through the axosomatic amplification mechanism¹². However, the possible role of active dendritic integration¹³⁻¹⁵ in further amplifying the sensory responses and sharpening the tuning curves of neurons¹⁶⁻¹⁹ is disregarded. Our findings show that dendrites of layer 4 spiny stellate neurons in the barrel cortex can generate local and global multi-branch N-methyl-D-aspartate (NMDA) spikes, which are the main regenerative events in these dendrites. In turn, these NMDA receptor (NMDAR) regenerative mechanisms can sum supralinearly the coactivated thalamocortical and corticocortical inputs. Using *in vivo* whole-cell recordings combined with an intracellular NMDAR blocker and membrane hyperpolarization, we show that dendritic NMDAR-dependent regenerative responses contribute substantially to the angular tuning of layer 4 neurons by preferentially amplifying the preferred angular directions over non-preferred angles. Taken together, these findings indicate that dendritic NMDAR regenerative amplification mechanisms contribute markedly to sensory responses and critically determine the tuning of cortical neurons.

To examine the active properties of layer 4 spiny stellate dendrites in the rodent barrel cortex and their role in synaptic integration, we first characterized layer 4 dendrites *in vitro* and then studied the contribution of active dendritic processing to sensory responses of these neurons *in vivo*.

The excitable properties of layer 4 spiny stellate dendrites *in vitro* were studied using focal synaptic stimulation of fluorescently identified dendrites while recording the somatic voltage^{18,20} (Fig. 1a). Linearly increasing the stimulus intensity resulted in an S-shaped input-output curve, with an abrupt amplitude jump, suggesting initiation of a dendritic spike (Fig. 1b-c). The average amplitude of dendritic spikes as recorded at the soma was 20.3 ± 2.7 mV and their average voltage threshold was 6.2 ± 1.1 mV ($n = 8$, 129 ± 33 μ m from soma). Blocking NMDAR channels by extracellular APV (2-amino 5-phosphonovalerate; 50 μ M) or intracellular MK801 through the recording pipette (see Methods for controls) completely abolished the spike, linearized the S-shaped input-output curve and significantly reduced the duration of the response (the half width was reduced by $50.3 \pm 5.8\%$, $P < 0.01$) (Fig. 1b-e). The extracellular APV had a larger average effect compared to intracellular MK801 (Fig. 1e), possibly owing to the fact that concentrations of MK801 did not fully equilibrate in distal dendrites where the focal stimulation occurred.

Unlike layer 5 pyramidal neurons, where dendritic NMDA spikes were mediated mostly by the NR2A subunit of the NMDAR channel²¹,

in layer 4 spiny stellate neurons both the NR2A (NVP-AAM077, 0.4 μ M) and NR2B (ifenprodil, 3 μ M) blockers did not significantly change the amplitude and threshold of the dendritic NMDA spikes (Fig. 1f-h; $P > 0.2$). These findings are consistent with a previous study that reported that NR2C subunits mediate the NMDA component of corticocortical excitatory postsynaptic potentials (EPSPs) in spiny stellate neurons²².

Next we used glutamate uncaging combined with specific blockers for voltage-gated calcium, sodium and NMDAR channels to further investigate the ionic mechanism mediating these dendritic spikes. Glutamate uncaging onto a single dendrite evoked a local spike that resembled the synaptically evoked dendritic spikes (Fig. 1i-j). Consecutive application of the specific voltage-gated sodium and calcium-channel blockers (1 μ M tetrodotoxin (TTX), 100 μ M Cd^{2+} and 100 μ M Ni^{2+}) did not change significantly the spike amplitude and threshold (Fig. 1i-k, $P = 0.2$). In contrast, consecutive application of APV blocked the spike completely (Fig. 1i-k; $n = 11$, $P < 0.01$). Taken together, our findings indicate that, similar to thin dendrites of layer 5 pyramidal neurons^{20,23,24}, NMDA spikes are the main regenerative events in dendrites of layer 4 spiny stellate neurons.

Our focal synaptic stimulation mostly activates corticocortical synaptic inputs as they constitute the majority of inputs to layer 4 spiny stellate dendrites²⁵. A second important source of inputs to these neurons (approximately 10% of all synapses) is the thalamocortical pathway, which carries the sensory input from the external world^{1,11,26}. Under physiological conditions the thalamocortical response is followed by a powerful feed-forward excitatory corticocortical activation originating from neighbouring layer 4 neurons²⁵. Thus, we next set out to examine the contribution of NMDAR-dependent dendritic regenerative mechanisms to the interaction between these two main excitatory inputs converging on layer 4 neurons. Thalamocortical responses were evoked by stimulating ventrobasal thalamic neurons while recording from somatotopically aligned layer 4 spiny stellate neurons (see Methods and Supplementary Figs. 1 and 2). Coactivation of a single predominantly corticocortical EPSP (average amplitude of 3.1 ± 0.6 mV), evoked by focal synaptic activation, with a train of thalamocortical EPSPs⁵ (5 pulses at 50 Hz) yielded an S-shaped curve. At the lower stimulus intensities, the two inputs summated sublinearly. As we gradually increased the thalamocortical stimulus intensity, an abrupt jump in the voltage response was observed, and the two inputs summated supralinearly (Fig. 2a-c, f). At just above threshold thalamocortical stimulus intensities, the paired response was $228.7 \pm 32.5\%$ greater than that expected from the linear summation of the thalamocortical and corticocortical EPSPs (Fig. 2b, c, f; $n = 12$). Extracellular APV or intracellular MK801 completely abolished this coincident amplification (Fig. 2a, f; the paired response was $86.8 \pm 18.2\%$ and $102.6 \pm 9.7\%$ of the expected arithmetic sum of the two individual responses for APV and MK801, respectively) and decreased the duration of the response (half width decreased by $49.0 \pm 4.3\%$; $n = 10$, $P < 0.01$). Similar results were obtained with

¹Department of Physiology, the Rappaport Faculty of Medicine & Research Institute, Technion-Israel Institute of Technology, Bat-Galim, Haifa 31096, Israel. ²Synaptic Physiology Section, National Institute of Neurological Disorders & Stroke, National Institutes of Health, Bethesda, Maryland 20892-3701 USA.

*These authors contributed equally to this work.

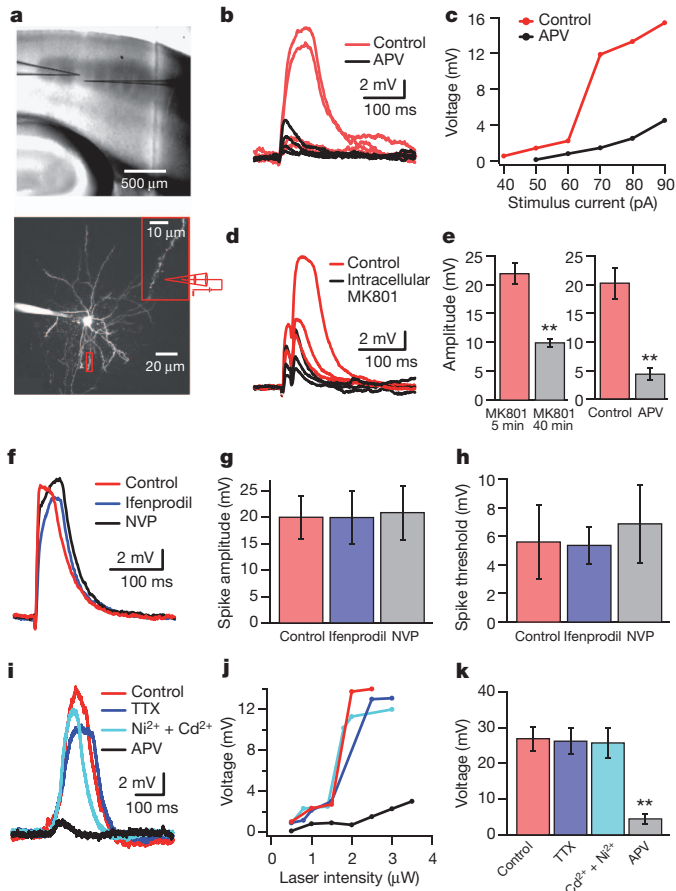


Figure 1 | NMDA spikes in layer 4 spiny stellate neurons. **a**, Experimental setup. Top panel, thalamocortical slice with two schematic electrodes (left, recording; right, stimulating). Bottom panel, layer 4 spiny stellate neuron loaded with alexa 633 (50 μ M). Inset, the stimulated dendritic branch (position indicated by a red rectangle) and a schematic drawing of the stimulating theta electrode. **b**, Somatic voltage recordings in response to gradual increase of the stimulus current at the dendrite, in control conditions and after NMDAR channels blockade with APV (50 μ M). **c**, Stimulus current–voltage relationship of the experiment shown in **b**. **d**, Same as **b**, except that the electrode contained MK801 (2 mM). Recordings were taken after 5 min (red) and 40 min (black). **e**, Average somatic amplitudes of the dendritic spike in control conditions and after NMDAR blockade with extracellular APV ($n = 8$) or intracellular MK801 ($n = 7$, after 40 min; $**P < 0.01$). **f**, Traces of NMDA spikes in control conditions, with ifenprodil (3 μ M) and followed by addition of NVP-AM077 (0.4 μ M). NVP, specific blocker of the NR2A subunit of the NMDAR. **g, h**, Averaged spike amplitude (**g**) and threshold (**h**). Colours are the same as in **f** ($n = 8$). **i**, Effect of voltage-gated sodium- and calcium-channel blockers on local spikes evoked by glutamate uncaging at a dendrite (160 μ m from soma). Spike in control conditions, with TTX (1 μ M), with consecutive addition of Ni^{2+} (100 μ M) and Cd^{2+} (100 μ M), and consecutive application of APV (50 μ M). **j**, Peak somatic voltage as a function of stimulus laser intensity (colours are the same as in **i**). **k**, The average amplitudes of the dendritic spike as recorded at the soma (colours are the same as in **i** and **j**) ($n = 11$, $**P < 0.01$ compared with control). Error bars, mean \pm s.e.m.

20-Hz and 100-Hz thalamocortical stimulation frequencies ($n = 6$; data not shown).

To mimic a distributed corticocortical activation pattern we activated the corticocortical inputs using a large extracellular stimulating electrode placed within the barrel that we recorded from. Similar to our previous results, pairing of a distributed corticocortical EPSP (average amplitude of 5.3 ± 0.89 mV) with thalamocortical EPSPs, evoked at gradually increasing stimulation intensities, resulted in a steep S-shaped input–output curve with supralinear summation of these two inputs above a threshold value (Fig. 2d–f). At just above threshold thalamocortical stimulus intensities, the response was 213.2

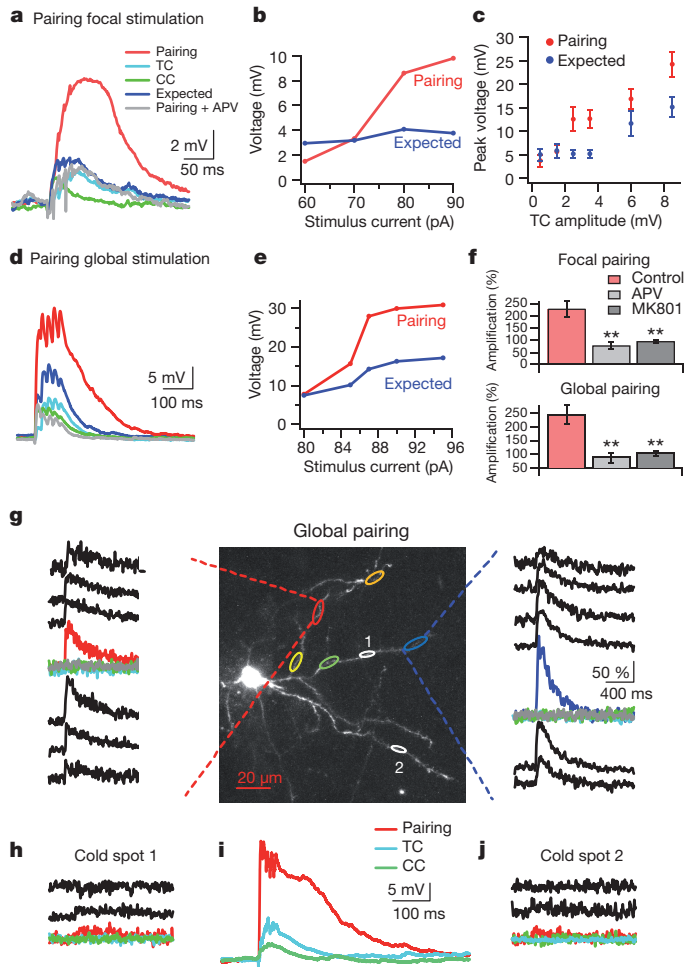


Figure 2 | Corticocortical and thalamocortical pairing of activity evokes local and multi-branch global dendritic NMDA spikes. **a**, Simultaneous activation of thalamocortical (TC) axons (100 Hz, 5 pulses) and corticocortical (CC) axons (1 pulse, focal stimulation) caused a large supralinear response (red) that was blocked by APV (grey). The expected arithmetic sum of the two individual responses is shown in blue. **b**, Voltage amplitude in response to pairing of corticocortical input (constant intensity) and thalamocortical input (increasing intensities) (red). Blue, expected arithmetic summed response. **c**, Peak average (mean \pm s.e.m.) paired and expected summed voltage responses as a function of the thalamocortical peak voltage amplitude ($n = 7$). **d, e**, Same as **a** and **b** but for global corticocortical stimulation (electrode was located approximately 200 μ m from the soma of the recorded neuron). **f**, Amplification (as a percentage of expected arithmetic summed response) in control conditions, with APV and with MK801. Data are presented for focal (top panel, $n = 12$) or global (bottom panel, $n = 10$) corticocortical activation ($**P < 0.01$ compared with control). Error bars, mean \pm s.e.m. **g**, Image of a spiny stellate neuron filled with OGB-1 (100 μ M) showing the location of five calcium hot spots (coloured ovals) during global pairing (red/blue) of thalamocortical (cyan) and corticocortical (green) activation. Spatial profiles of the red (left panel) and blue (right panel) hot spots are shown. The blue and red traces were recorded at the peak locations of the spots, and the black traces were recorded at adjacent sites with distance steps of 3 to 5 μ m between consecutive traces. **h–j**, Spatial profiles of two ‘cold spots’ (white ovals in **g**) and the corresponding somatic voltage recordings during the pairing protocol (**i**).

$\pm 25.5\%$ greater than the calculated arithmetic sum of the two individual responses (Fig. 2e–f, $n = 10$). This amplification was blocked by extracellular APV or intracellular MK801 (Fig. 2d, f; $n = 8$, the amplitude of the paired response decreased to $68.8 \pm 18.2\%$ relative to the calculated arithmetic sum of the individual responses, and half width decreased to $48.8 \pm 6.5\%$, $P < 0.01$).

The intracellular block of NMDAR channels indicated mainly a postsynaptic effect in the recorded neuron rather than a recurrent

network effect (see controls in Methods and Supplementary Figs. 3 and 4).

To understand better the dendritic events underlying the supralinear summation in the focal and global pairing protocols, we carried out simultaneous calcium imaging recordings in dendrites of the activated layer 4 neurons. During the global and focal pairing, calcium imaging revealed intense dendritic ‘hot spots’ (Fig. 2g–j and Supplementary Fig. 5). During the focal pairing, calcium transients were localized to the activated sites and reached an average amplitude of $170 \pm 30.5\%$ ($\Delta F/F$) which was significantly larger than the corticocortical-evoked calcium transients ($30 \pm 7\%$, $P < 0.01$) and thalamocortical-evoked transients alone (undetectable, below the noise level) ($n = 4$ neurons; Supplementary Fig. 5). Similar results were obtained when the focal synaptic stimulation was replaced with focal glutamate uncaging ($n = 6$; Supplementary Fig. 6).

In the case of global pairing we observed multiple calcium hot spots in several dendrites (Fig. 2g, i). On average we observed 3.8 ± 0.6 calcium hot spots per neuron when scanning approximately 30% of the dendritic tree. The average size of the maximal calcium hot zone ranged between 9 and $30 \mu\text{m}$ (average $15 \pm 1.4 \mu\text{m}$) and their average peak amplitude during the pairing was $135 \pm 14\%$ ($n = 18$ spots). During thalamocortical activation alone, calcium transients were undetectable, as was the case in most instances of corticocortical activation (Fig. 2g; 14 out of the 18 cases). In the 4 cases in which we observed calcium transients during corticocortical activation, the average peak calcium transient was $34 \pm 11.5\%$. The calcium transients evoked by the pairing protocol were abolished altogether by APV (Fig. 2g; $n = 15$ spots). Similar multi-branch NMDA spikes were also observed in layer 4 pyramidal neurons (Supplementary Fig. 7). Interestingly, in contrast to previously reported data in layer 2 neurons of the visual cortex²⁷ where calcium hot spots originated from activation of single inputs, in this study the calcium hotspots were found to extend over larger dendritic segments, indicating supralinear interactions between neighbouring synapses.

Computer simulations succeeded in reproducing the experimental results of NMDA spike generation and their accompanying calcium profiles during both focal and global activation patterns (Supplementary Figs 8 and 9). Simulations show that during global multi-branch NMDA spikes, the voltage profile was relatively homogenous across the neuron, whereas the calcium profile was highly non-homogenous, showing calcium hot spots in different dendritic segments (Supplementary Fig. 9a, d). Our simulation indicated that the global multi-branch NMDA spike resulted from regenerative interactions between closely spaced synapses as well as from long-range inter-branch interactions between more distant synapses.

To investigate directly the contribution of NMDAR-dependent dendritic regenerative mechanisms to tuning of sensory responses, we turned to *in vivo* experiments. More specifically, we examined the hypothesis that NMDAR-dependent dendritic regenerative mechanisms can serve to sharpen the angular tuning curves^{5,28} of barrel cortex layer 4 neurons by comparing the whisker-evoked responses to deflection in 8 cardinal angular directions (in 45° increments) in control conditions and after blockade of the postsynaptic NMDAR in the recorded neuron with either intracellular MK801 or membrane hyperpolarization. Whole-cell patch-clamp recordings from layer 4 neurons were carried out *in vivo* from an a priori mapped principal barrel (mapped by intrinsic optical imaging) (Fig. 3a and Supplementary Fig. 10). The recorded neurons and their relationship to the barrel boundaries were identified histologically at the end of each experiment (see Methods and Supplementary Fig. 10).

Consistent with previous studies⁵, we found that responses of layer 4 neurons were tuned to the angular direction of the whisker deflection in the sub- and suprathreshold range (Figs 3 and 4). The average selectivity index was 0.64 ± 0.03 for subthreshold responses. The angular tuning maps remained stable throughout the length of the recording when the recording electrode contained control solution

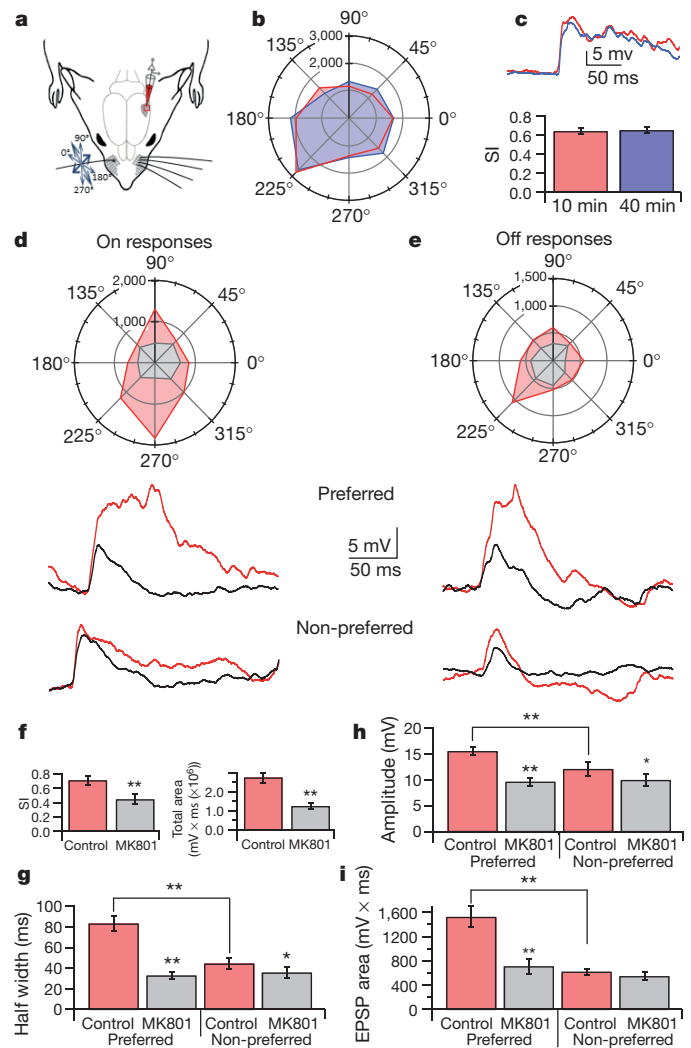


Figure 3 | The role of NMDAR-dependent dendritic regenerative responses in angular tuning of layer 4 neurons *in vivo*. **a**, Whole-cell patch-clamp recordings were carried out from layer 4 cells *in vivo* while deflecting the principal whisker in eight cardinal directions (see Methods). **b**, Polar plot showing average EPSP area (in $\text{mV} \times \text{ms}$) of the ‘on’ responses to whisker deflection in 8 directions (every 45°) obtained 2 to 12 min (red) and 30 to 40 min (blue) after whole-cell break with control pipette solution. **c**, Top, response to the preferred direction (225°) in the first 10 min and after 40 min. Bottom, average selectivity index (SI) calculated 10 and 40 min after whole-cell break ($n = 6$). **d**, Top, polar plot showing average on responses obtained 2 to 8 min (red) and 30 to 36 min (grey) after whole-cell break with an electrode containing MK801 (4 mM). Bottom, example traces of on responses to the preferred (upper traces) and non-preferred (lower traces) directions, during control recordings (red) and after 32 min with MK801 (black). **e**, Same as **d** but for the off responses (same neuron as in **d**). **f**, Average SI (left panel) of neurons in control conditions (first 10 min of recording) and with intracellular MK801 (after 40 min). Average area (right panel) of the angular tuning maps in control conditions (first 10 min of recording) and with intracellular MK801 (after 40 min). **g–i**, Average EPSP half width, amplitude and area of the subthreshold responses to preferred and non-preferred directions in control conditions (first 10 min of recording) and with intracellular MK801 (after 40 min). In all measurements the preferred and non-preferred directions were the directions of whisker deflection with the largest and smallest responses, respectively. $n = 13$, $*P < 0.05$; $**P < 0.01$. Error bars, mean \pm s.e.m.

($102 \pm 7\%$ after 40 min of recordings, $n = 6$; Fig. 3b, c). In contrast, angular tuning was significantly affected when MK801 (2–4 mM) was present in the recording electrode. Following intracellular NMDAR blockade, the selectivity index dropped significantly from 0.71 ± 0.06 in the first 10 min of the recording to 0.44 ± 0.07 after 30 to 40 min from the break to the whole-cell configuration ($P < 0.01$, $n = 13$;

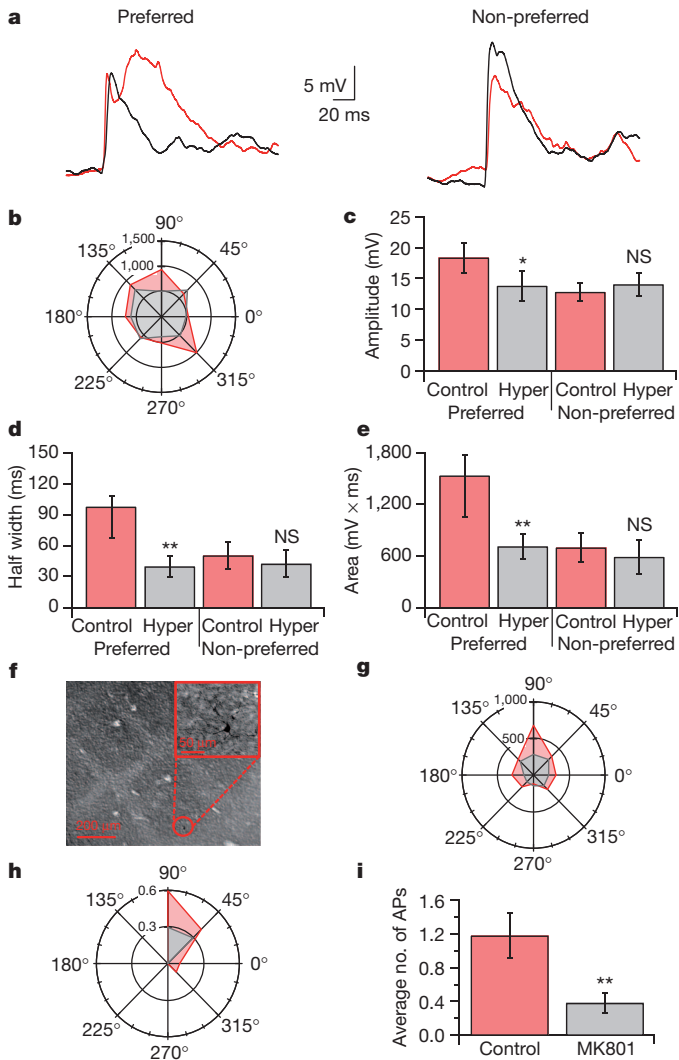


Figure 4 | Effect of hyperpolarization on the angular tuning responses of layer 4 neurons *in vivo* and the effect of MK801 on angular tuning of suprathreshold responses. **a**, Examples of traces of on responses to whisker deflection in the preferred (left panel) and non-preferred (right panel) directions in control (red) and after membrane potential hyperpolarization by 15 mV (black). **b**, Angular tuning maps (area measured in mV × ms) of the on subthreshold responses to whisker deflection in eight different directions in resting membrane potential (control, red) and after membrane potential hyperpolarization by 15 mV (grey). **c–e**, The average (mean ± s.e.m.; $n = 6$) EPSP amplitude (**c**) half width (**d**) and area (**e**) of the preferred and non-preferred responses in resting membrane potential (control), and after membrane potential hyperpolarization (Hyper) by 15 mV. **f**, Tangential view of the biocytin-stained spiny stellate neuron and its location according to the cytochrome-oxidase-dense regions typical to layer 4 barrels. **g, h**, Angular tuning maps of the on subthreshold responses (**g**) and the on suprathreshold action-potential firing responses (**h**) to whisker deflection in eight different directions in the presence of intracellular MK801 in the first 10 min (control, red) and after 40 min (grey). **i**, The average number (± s.e.m.; $n = 6$) of action potentials fired during the preferred angular direction in the presence of intracellular MK801 in the first 10 min (control, red) and after 40 min. The subthreshold maps depict the average EPSP area, and the suprathreshold map depicts the average number of action potentials during the on responses. * $P < 0.05$; ** $P < 0.01$. APs, action potentials; NS, not significant.

Fig. 3d–f and Supplementary Fig. 11). The sharp drop in angular tuning selectivity was caused by the fact that the NMDAR preferentially contributed to the area, half width and amplitude of the responses to the preferred angular deflection compared with the non-preferred angles, which were affected as expected from *in vitro* data⁸ (Fig. 3d–i). The large contribution of NMDAR (59.8% and 49.6% of

the EPSP half width and area, respectively) indicated the participation of NMDAR dendritic regenerative mechanism in amplifying the preferred responses. Consistent with participation of regenerative dendritic NMDAR responses, hyperpolarization of the membrane potential by approximately 15 mV caused a significant decrease in the responses to the preferred direction (Fig. 4a–e).

For the suprathreshold range, we observed a sharp reduction in the average number of action potentials in the preferred angular direction with intracellular blockade of NMDAR channels. The average number of action potentials in the preferred direction dropped from 1.18 ± 0.27 per stimulus in the first 10 min of recording to 0.38 ± 0.13 after 30 to 40 min of recording with intracellular MK801 (67.8%, $n = 6$, $P < 0.01$, Fig. 4f–i). Analysis of suprathreshold responses was limited to the preferred angles owing to the small number of action potentials evoked by non-preferred angles already under control conditions.

Similar to its contribution in angular tuning responses, NMDAR dendritic regenerative activation also significantly contributed to sensory responses in layer 4 neurons evoked by artificial whisking (see Supplementary Fig. 12).

To understand further the contribution of NMDAR-dependent dendritic mechanisms to shaping the angular tuning responses of layer 4 neurons, we simulated thalamocortical and feed-forward excitatory and inhibitory responses in a multi-compartmental spiny stellate cell model (Supplementary Fig. 13a). Our simulations show that dendritic NMDAR regenerative properties crucially contributed to angular tuning. The preferred selectivity was determined by the input bias, which is amplified further by regenerative dendritic NMDAR responses (Supplementary Fig. 13). Indeed, the selectivity index dropped to the level represented by the presynaptic excitatory bias across a wide range of stimulation intensities when the NMDAR channels were excluded (Supplementary Fig. 13d, f, g).

In conclusion, our data indicate that dendritic NMDARs in layer 4 neurons can facilitate a spectrum of dendritic regenerative events ranging from graded amplification to full-blown local and global dendritic NMDA spikes²⁹. This dendritic regenerative mechanism has a role in shaping the responses to whisker sensing, and is crucial for the formation of angular tuning responses in layer 4 neurons.

Dendritic NMDAR regenerative amplification can carry several ‘physiological benefits’, including the ability to drive the neuron by a smaller number of thalamocortical inputs and a reduction in the number of biased thalamic inputs⁵ required to generate sharp and stable tuning curves. We propose that the axonal amplification mechanism of biased inputs³⁰ suggested previously is combined with dendritic amplification mechanisms to efficiently translate small biases in the input profile to sharply tuned output responses.

METHODS SUMMARY

For the *in vitro* experiments, thalamocortical slices were prepared from CD-1 mice. Whole-cell patch-clamp recordings, focal and global synaptic stimulation calcium imaging and glutamate uncaging were carried out with visually identified layer 4 spiny stellate neurons using standard techniques^{21,23}.

For *in vivo* experiments, whole-cell patch-clamp recordings were performed using urethane-anaesthetized Wistar rats. The principal whisker was identified using intrinsic optical imaging and activated using either artificial whisking evoked by stimulating the buccal branch of the facial motor nerve or by passive whisker deflection in eight cardinal directions using a pair of crossed piezoelectric bimorphs⁵.

Simulations were conducted on a multi-compartmental spiny stellate neuron with realistic morphology, voltage-gated channel distribution and parameters of synaptic activation.

Received 20 May; accepted 27 July 2012.

Published online 2 September 2012.

1. Benshalom, G. & White, E. L. Quantification of thalamocortical synapses with spiny stellate neurons in layer IV of mouse somatosensory cortex. *J. Comp. Neurol.* **253**, 303–314 (1986).

2. Binzegger, T., Douglas, R. J. & Martin, K. A. A quantitative map of the circuit of cat primary visual cortex. *J. Neurosci.* **24**, 8441–8453 (2004).
3. Hubel, D. H. & Wiesel, T. N. Receptive fields, binocular interaction and functional architecture in the cat's visual cortex. *J. Physiol.* **160**, 106–154 (1962).
4. Woolsey, T. A. & Van der Loos, H. The structural organization of layer IV in the somatosensory region (S1) of mouse cerebral cortex. The description of a cortical field composed of discrete cytoarchitectonic units. *Brain Res.* **17**, 205–242 (1970).
5. Bruno, R. M., Khatri, V., Land, P. W. & Simons, D. J. Thalamocortical angular tuning domains within individual barrels of rat somatosensory cortex. *J. Neurosci.* **23**, 9565–9574 (2003).
6. Wang, H. P., Spencer, D., Fellous, J. M. & Sejnowski, T. J. Synchrony of thalamocortical inputs maximizes cortical reliability. *Science* **328**, 106–109 (2010).
7. Bruno, R. M. & Sakmann, B. Cortex is driven by weak but synchronously active thalamocortical synapses. *Science* **312**, 1622–1627 (2006).
8. Gil, Z., Connors, B. W. & Amitai, Y. Efficacy of thalamocortical and intracortical synaptic connections: quanta, innervation, and reliability. *Neuron* **23**, 385–397 (1999).
9. Stratford, K. J., Tarczy-Hornoch, K., Martin, K. A. C., Bannister, N. J. & Jack, J. J. B. Excitatory synaptic inputs to spiny stellate cells in cat visual cortex. *Nature* **382**, 258–261 (1996).
10. Sarid, L., Bruno, R., Sakmann, B., Segev, I. & Feldmeyer, D. Modeling a layer 4-to-layer 2/3 module of a single column in rat neocortex: interweaving *in vitro* and *in vivo* experimental observations. *Proc. Natl Acad. Sci. USA* **104**, 16353–16358 (2007).
11. Alonso, J. M., Usrey, W. M. & Reid, R. C. Precisely correlated firing in cells of the lateral geniculate nucleus. *Nature* **383**, 815–819 (1996).
12. Priebe, N. J. & Ferster, D. Inhibition, spike threshold, and stimulus selectivity in primary visual cortex. *Neuron* **57**, 482–497 (2008).
13. Johnston, D., Magee, J. C., Colbert, C. M. & Christie, B. R. Active properties of neuronal dendrites. *Annu. Rev. Neurosci.* **19**, 165–186 (1996).
14. Magee, J., Hoffman, D., Colbert, C. & Johnston, D. Electrical and calcium signaling in dendrites of hippocampal pyramidal neurons. *Annu. Rev. Physiol.* **60**, 327–346 (1998).
15. Häusser, M., Spruston, N. & Stuart, G. J. Diversity and dynamics of dendritic signaling. *Science* **290**, 739–744 (2000).
16. Poirazi, P. & Mel, B. W. Impact of active dendrites and structural plasticity on the memory capacity of neural tissue. *Neuron* **29**, 779–796 (2001).
17. Branco, T. & Häusser, M. The single dendritic branch as a fundamental functional unit in the nervous system. *Curr. Opin. Neurobiol.* **20**, 494–502 (2010).
18. Polsky, A., Mel, B. W. & Schiller, J. Computational subunits in thin dendrites of pyramidal cells. *Nature Neurosci.* **7**, 621–627 (2004).
19. Archie, K. A. & Mel, B. W. A model for intradendritic computation of binocular disparity. *Nature Neurosci.* **3**, 54–63 (2000).
20. Schiller, J., Major, G., Koester, H. J. & Schiller, Y. NMDA spikes in basal dendrites of cortical pyramidal neurons. *Nature* **404**, 285–289 (2000).
21. Polsky, A., Mel, B. & Schiller, J. Encoding and decoding bursts by NMDA spikes in basal dendrites of layer 5 pyramidal neurons. *J. Neurosci.* **29**, 11891–11903 (2009).
22. Fleidervish, I. A., Binshtok, A. M. & Gutnick, M. J. Functionally distinct NMDA receptors mediate horizontal connectivity within layer 4 of mouse barrel cortex. *Neuron* **21**, 1055–1065 (1998).
23. Larkum, M. E., Nevian, T., Sandler, M., Polsky, A. & Schiller, J. Synaptic integration in tuft dendrites of layer 5 pyramidal neurons: a new unifying principle. *Science* **325**, 756–760 (2009).
24. Major, G., Polsky, A., Denk, W., Schiller, J. & Tank, D. W. Spatiotemporally graded NMDA spike/plateau potentials in basal dendrites of neocortical pyramidal neurons. *J. Neurophysiol.* **99**, 2584–2601 (2008).
25. Stratford, K. J., Tarczy-Hornoch, K., Martin, K. A., Bannister, N. J. & Jack, J. J. Excitatory synaptic inputs to spiny stellate cells in cat visual cortex. *Nature* **382**, 258–261 (1996).
26. White, E. L. & Rock, M. P. Three-dimensional aspects and synaptic relationships of Golgi-impregnated spiny stellate cell reconstructed from serial thin sections. *J. Neurocytol.* **9**, 615–636 (1980).
27. Jia, H., Rochefort, N. L., Chen, X. & Konnerth, A. Dendritic organization of sensory input to cortical neurons *in vivo*. *Nature* **464**, 1307–1312 (2010).
28. Kremer, Y., Leger, J. F., Goodman, D., Brette, R. & Bourdieu, L. Late emergence of the vibrissa direction selectivity map in the rat barrel cortex. *J. Neurosci.* **31**, 10689–10700 (2011).
29. Schiller, J. & Schiller, Y. NMDA receptor-mediated dendritic spikes and coincident signal amplification. *Curr. Opin. Neurobiol.* **11**, 343–348 (2001).
30. Priebe, N. J. & Ferster, D. Direction selectivity of excitation and inhibition in simple cells of the cat primary visual cortex. *Neuron* **45**, 133–145 (2005).

Supplementary Information is available in the online version of the paper.

Acknowledgements We thank Y. Schiller and G. Major for their helpful comments and discussions on the manuscript. We thank A. Korngreen and C. de Kock for help with NeuroLucida reconstructions, U. Dubin for help in programming the stimulus and analysis programs, O. Schiff for help with Igor software and R. Azouz for help with the passive stimulus. We thank I. Reiter for her technical help, particularly with histology. We also thank R. Bruno for sharing his knowledge of *in vivo* patch clamp recordings. This study was supported by the Israel Science Foundation (ISF) and the Rappaport Foundation (J.S.).

Author Contributions M.L. and L.G. performed the *in vivo* experiments and S.R. carried out the *in vitro* slice experiments and helped with analysis. A.P. performed the computer simulations. J.S. designed the study, assisted in the experiments, carried out the analysis and prepared the manuscript. M.L. also participated in the manuscript preparation.

Author Information Reprints and permissions information is available at www.nature.com/reprints. The authors declare no competing financial interests. Readers are welcome to comment on the online version of the paper. Correspondence and requests for materials should be addressed to J.S. (Jackie@bx.technion.ac.il).